

# Numerical Planing Vessel Approximation

KIRSTEN ODENDAAL  
TU Delft

April 19, 2020

## I. INTRODUCTION

In the past hydrodynamic characteristics of planing vessels have been studied with many experiments in towing tanks, from which there have been attempts to develop analytical relations for the approximation of hydrodynamic forces acting on planing vessels such as Savitsky's Method. However in the last decade CFD studies have become more relevant in the design process of planing vessels and CFD is even becoming a substitute for towing tank tests. Therefore multiple methods have been developed of which some are based on simplification such as reducing the 3D problem to the solution of a series of 2D potential flow problems on the sections. This 2D to 3D transformation can simply be related using a time-length domain relation as seen in formulation (1).

$$x = U \cdot t \quad (1)$$

A visual representation of the this formulation can be seen in figure (1), where a dropping wedge in the time domain is converted to the time rate of change over the length of the planing hull.

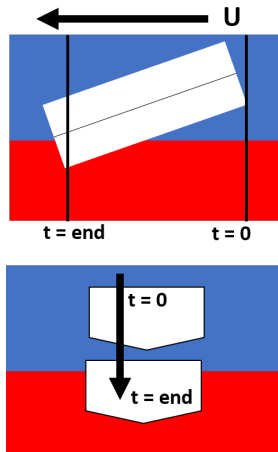


**Figure 1:** General  $x-t$  visual representation

To compare the validity and differences between CFD and analytical methods, this paper will review the results of the hydrodynamic calculations of a planing vessel with a CFD method, Savitsky's Method and finally Von Karman's Method.

## II. GEOMETRY

### i. Savitsky's Method

To determine the key parameters of the vessel geometry, Savitsky's hydrodynamic design of planing hulls was consulted [2]. Savitsky suggested that the hydrodynamic characteristics of prismatic planing surfaces were a close representation of planing craft. Using this approximation, key formulations and empirical results were combined to describe the drag, equilibrium trim, and wetted keel length, and depth of transom.

The main advantage of implementing Savitsky's methods is due to the relative computational ease these formulations are able to provide. It also offers a easy validation check for the

lift and drag forces. Thus, using the computational general case procedure for hydrodynamic performance, the key initial design parameters for the study were determined. These key parameters can be seen labeled in figure (2).

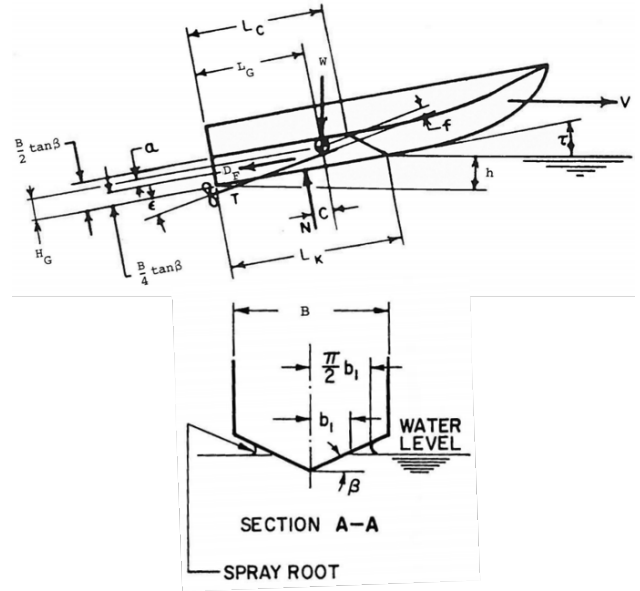


**Figure 2:** Planing vessel general schematic and parameters [2]

Where, the parameters of interest are;  $\tau$ , the trim angle of the keel.  $d$ , draft of the keel at the transom.  $L_k$ , the wetted keel length.  $\beta$ , the inclined dead rise angle of the hull.  $b$ , the beam of the craft. To remain consistent with Savitsky's, the same vessel dimensions were implemented and analyzed. This will not only allow for the determination of the key wedge parameters, it will also give a valid analytical comparison result to check with the final CFD results. Therefore a resulting output summary of all parameters can be seen in table 1.

**Table 1:** Summary of vessel initial parameters

Initial Vessel Parameters		
Length, $L$	m	18.00
Beam, $b$	m	4.00
DR, $\beta$	$^\circ$	15.00
Velocity, $U$	m/s	15.42
Froude <sub>b</sub> , $Fn_b$	-	2.46
trim, $\tau$	$^\circ$	4.00
Wet Keel, $L_k$	m	14.92
Keel depth, $d$	m	1.05
Lift Force, $F_L$	N	2.91e5
Drag Force, $F_D$	N	2.05e4

All relevant formulations and empirical results can be found in [2]. However, one key parameter that requires further discussion is the Froude number. Since the planing hull does not typically have a constant water line length due to lift, the traditional representation of the Froude number must be reconsidered. Therefore,

the implementation of a Froude with respect to the beam can be substituted instead.

$$Fn_b = \frac{U}{\sqrt{g \cdot b}} \quad (2)$$

This form of the the Froude number is still capable of maintaining its dimensionless advantage. It should be noted that the empirical equations of Savitsky for  $L_k$  are only valid for a speed coefficient of two or greater ( $Fn_b > 2$ ), deadrise less than 15 degrees ( $\beta < 15$ ), and trim less than or equal to 4 degrees ( $t \leq 4^\circ$ ).

## ii. Mesh Generation

Having determined the full parameters of the vessel in question, a conversion from the 3-dimensional space can be made to the 2-dimensional wedge space. This can be simply be done by changing the orientation of the parameters through use of the trim angle and trigonometry. Thus, the required start height, end depth, and drop velocity can be determined using the following relations,

$$H_{drop} = (L - L_k) \cdot \tan(\tau) \quad (3)$$

$$d_{drop} = d \cdot \cos(\tau) \quad (4)$$

$$V_{drop} = U \cdot \sin(\tau) \quad (5)$$

From these parameters the time required for the wedge to fall through the space and fluid can be determined respectively,

$$t_{impact} = H_{drop} / V_{drop} \quad (6)$$

$$t_{fluid} = d_{drop} / V_{drop} \quad (7)$$

A detailed summary of these wedge parameters can be seen in table 2

**Table 2:** Summary of wedge initial parameters

Wedge Parameters		
Height above FS, $H_{air}$	m	0.21
Height below FS, $d_{fluid}$	m	1.05
Drop velocity, $V_{drop}$	m/s	1.08
Total drop time, $t_T$	s	1.16
Impact time, $t_{impact}$	s	0.19
Fluid time, $t_{fluid}$	s	0.97

## iii. Mesh Domain Determination

With these complete set of parameters the full domain of Analysis can be completed. To save computational demand a symmetric body will be evaluated.

The domain will be represented as a function of the vessels beam. This will allow for a systematic approach in determining the domain size. Ultimately due to the implemented boundary conditions of the domain for the fluid and air cannot be too small. If the fluid does not have sufficient room to displace itself, the interaction between the wedge, air, and fluid can greatly skew the results. This can have a drastic effect on the pressure experienced on the wedge which in turn will inflate the expected force values. However, if the domain is too large, the excess elements can greatly increase the required computational demand. Thus, a fine medium between the two is required. This was essentially achieved through a trial and error methodology.

$$Width = 3 \cdot b \quad (8)$$

$$Height = 3 \cdot b \quad (9)$$

$$Area = 30.92m^2$$

Where the domain height is decomposed into two equally spaced areas for both the fluid and air regions respectively. As such, the domain area can be determined as the total square domain minus the area related to the wedge.

## iv. Parabolic Deadrise Representation

The initial parameters are established for a constant deadrise of 15°. However, this case with a constant angle has been extensively evaluated in previous wedge/planing vessel research. Therefore, the implementation of a parabolic representation of the dead rise angle is instead considered. To maintain the validity of the determined vessel parameters, this constantly changing dead rise has an averaged angle of 15°.

$$Y_{poly} = -0.020704 \cdot b^2 + 0.311407 \cdot b \quad (10)$$

To determine the above polynomial representation, it was crucial that the polynomial curve can be simply represented as an interpolated spline function. This is due to the mesh creation in general. The meshing software, GMSH, is only able to represent curvatures using point intersecting interpolated splines. Therefore, a comparison between the 2nd order polynomial and the interpolated spline can be seen in figure (3). From this figure it

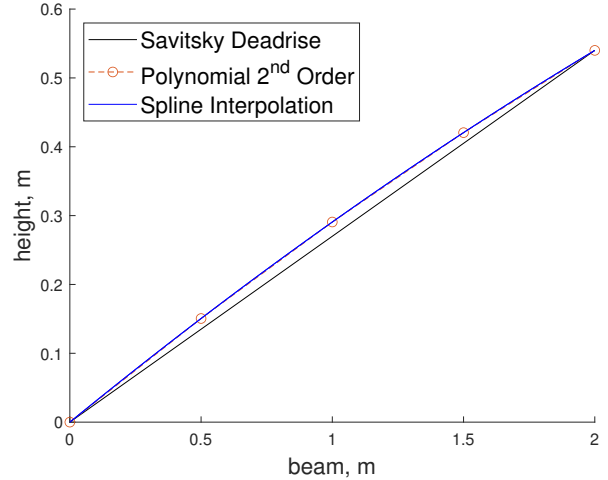


**Figure 3:** Parabolic curve comparison

can be seen that using 5 points, the spline and the polynomial function have very good similarity between the two. Furthermore, the relative error between the curves show that the maximum deviation is on the order of  $10^{-10}$ . Thus, equation (10) will confidently be used to represent the wedge geometry.

## v. Geometrical Similarity

To ensure that the meshes were geometrically similar, and element scale factor was implemented. A factor of  $\sqrt{2}$  was used. Implementing this factor allowed for 6 different meshes ranging from the coarsest mesh with 3,649 elements to the most fine with 102,277. The meshes were arbitrarily chosen so that the final mesh size ranged close to the 100,000 element marker. This value was chosen to have a reasonable computationally demanding solution, allowing for a modest final run time. A summary of all the meshes can be found in table 3.

Where the average element size can be determined using the

**Table 3:** Summary of wedge mesh parameters

Triangular Mesh Properties		
Mesh	Element #	Element Size
$h_6$	3649	0.0921
$h_5$	6918	0.0669
$h_4$	13510	0.0478
$h_3$	26303	0.0343
$h_2$	51133	0.0246
$h_1$	102277	0.0174

approximation,

$$h_i = \sqrt{\frac{Area}{Element_i}} \quad (11)$$

It should be noted however, that while the meshes were refined using a scaling factor, not all triangular mesh elements were of the same size. During the meshing procedure, mesh elements below the wedge were manual refined by a further factor of 20. This was to ensure that the physics was properly captured in this region, allowing for a more accurate analysis of the hydrodynamic forces occurring on the wedge. From figure (4), a comparison between the the coarsest and finest meshes can be clearly seen.

### III. CFD AND VISUALIZATION

#### i. Parameter Selection

Before the wedge program can be implemented, the initial inputs must be established to ensure that the numerical results and simulations are accurately reflected. This is achieved directly through the modification and justification of the solver type, artificial diffusion, CFL number, and time stepping.

1. ODE-Solver: The solver type plays a crucial role in the accuracy and stability of the numerics. During the solution determination phase three different solvers were ultimately tested and analyzed. The ode21; Implicit Backwards Euler and the ode32, implicit generalized-alpha. From the results it was quickly determined that ode45 gave very oscillatory results early in the initialization phase as compared to the other solutions. However, the results themselves were of an increased 2nd order of accuracy. Whereas the ode21 gave an inherently stable solution, but suffered from a 1st order accurate result. Ultimately, it was determined for the higher mesh sizes, stability will be of crucial importance. As such the backward Euler was implemented for all meshes.
2. Level Set and Navier-Stokes Artificial Diffusion: These parameters consist of added diffusion terms required to add stabilization criteria to the Pressure Stabilized Petrov-Galerkin method. The residual based artificial diffusion increases accuracy however, as consequence makes solving the equations more difficult. Whereas, inconsistent diffusion aids with the solver performance. Too much diffusion in the system can lead to non-physical solutions. Therefore, these parameters must be kept as low as possible. While there is no explicitly theory to exactly setting these parameters, a trial and error methodology was implemented to achieve smooth and accurate results.
3. CFL number and time-step gain: The CFL relates the ratio of velocities between how many elements a particle travels

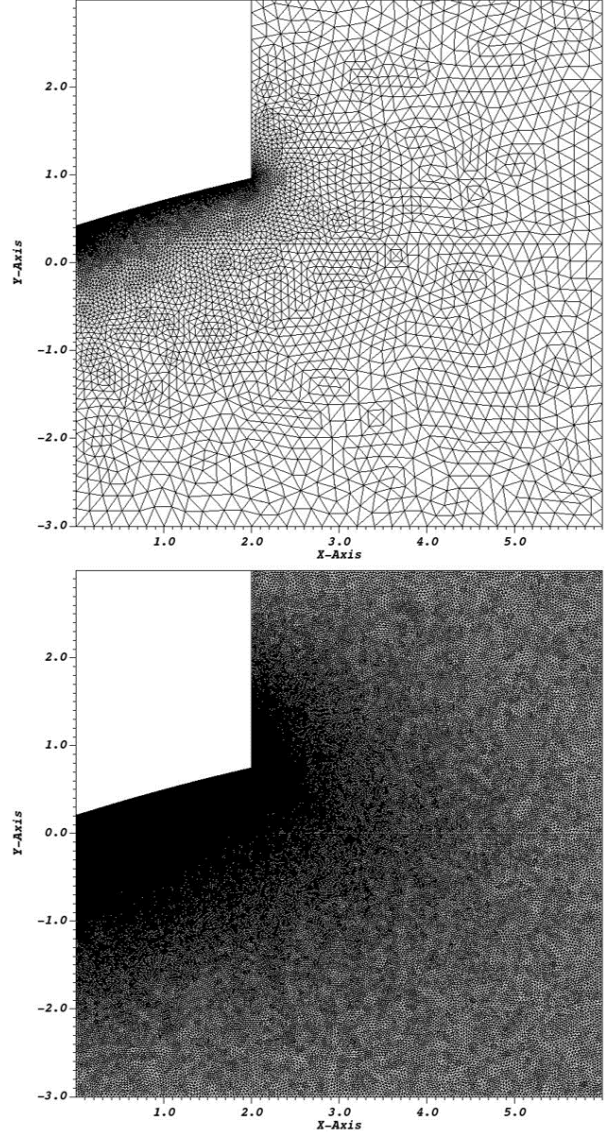


**Figure 4:** Mesh element comparison Top: 3,649 Bottom: 102,277

per time-step.

$$CFL = \max \left( \frac{|\mathbf{u}| \cdot \Delta t}{h} \right)_{x \in \Omega} \quad (12)$$

For implicit methods the time-step is limited in terms of accuracy for very large values. Thus the CFL target value should range between 1-2 for an optimal efficiency. To ensure this CFL target can be achieved for each target, the time-step must constantly be adjusted. This is done through a time-step gain parameter.

$$\Delta t^{n+1} = \Delta t^n \left( \frac{cfl - target}{cfl} \right)^{dt-gain} \quad (13)$$

This gain controls the responsiveness to which the CFL changes and ranges between 0 and 1. Where 0 is no change and 1 is considered instantaneous adaptation. This in many

cases is known as a dead-beat controller and is too responsive. Therefore, a gain between these parameters was established to ensure a sound medium in terms of adaptivity.

Using these justifications, along with extensive trial and error the following summary of the input wedge parameters used in the CFD analysis can be seen in table 4.

**Table 4:** Summary of wedge input parameters

Wedge Program Input Parameters			
Parameter	Value	Parameter	Value
refine	0	newton-tolerance	0.001
order	1	newton-itermax	10
ode-solver	21	velocity	1.08
t-final	1.16	viscosity	0
cfl-target	1.1	LS-width	3
dt-gain	0.5	LS-ad-rb	0.4
time-step	0.01	LS-ad-ic	0.3
dt-min	0.0001	NS-ad-rb	0.4
dt-max	1	NS-ad-ic	0.1
lead	20	alpha-reg	100
linear	0.001	dt-vis	0.01
linear-itermax	500		

## ii. Parameter Uncertainties

It should be noted that while it is believed these parameters produce an accurate representation of the corresponding wedge physics, other parameters may have allowed for either a more efficient and/or accurate solution.

The first to mention is the order parameter. This establishes the gluing form between the Galerkin shape functions. The one represents a first order linear function gluing method. This is one of the most basic methods and resolves straight domains without any discontinuities between each element. However, this method is inherently incorrect in the following wedge analysis. The reason for this is because the instead of a linear deadrise angle, a polynomial is instead used. Therefore, it can be expected that there maybe be several kinks between the elements in this region which can lead to slight inaccuracies and/or difficulties during the numeric solving. Thus, a better representation of the glue elements would be to use a 2nd order poly function. In the following analysis this was not used due to the extra computational demand required by the system to solve these sets of parameters. However, as mesh size decreases, this problem should become less of an issue.

Another parameter that could be further investigated in the future is the lead time. This value establishes a artificial time amount for the solution to initialize and stabilize the numerical solution. However, if lead time is too long, then the system will unnecessarily increase the required amount of calculations. this in turn increases the computational demand and thus the time for each simulation to complete. As such, it might be more efficient to shrink the lead time to the shortest possible duration for the much larger mesh sizes.

Finally, for the smaller mesh sizes, it was a noticed that the iterations of the solvers were never exceeded. However, when the mesh size increased the demand and complexity of the numerics increased resulting in certain periods of non-convergence. While the general physics of the problem converged adequately the other parameters involving the level-set diffusion had more

difficulty. As such it can be assumed that additional study should be invested into the optimal diffusion settings which will provide an optimal solution for most all mesh sizes. This may also be accompanied through a look into the solver tolerance and iteration margins, which were not changed during the course of the study.

## iii. Computational Processing

Having established all necessary criteria and parameters, the wedge program could be implemented for each associated mesh family. For the four coarsest meshes, a computer with with an Intel(R) i7 processor operating on 4 Cores was used to run each simulation. The results were generally completed within an acceptable time range of 25 minutes (3649 elements) to 3 hours (26,303 elements). However, any mesh size smaller than this would take an extraordinary long time. As such, a TU Delft cluster was applied to the final two meshes for the sake of computational time relief. Each job had access to 12 cores, thus allowing for an approximate 3x faster computational speed.

## iv. Wedge Analysis

For each result, the open source visualization tool, visit, was implemented to organize and analyze the data in a functional form. As a result, the wedge simulation computations were visually represented for the most refined mesh size. Figures containing the fluid boundary, pressure, velocity magnitude and velocity vectors were analyzed independently can be seen in figures (5), (6), (7), and (8) respectively.

From the flow boundary solution, a clear representation of the fluids and their division can be seen. Where, blue indicates the air and red is the fluid. In figure (5), the fluid pile-up can clearly be seen in the zoomed region. This pile-up is generally quite similar to other wedge drop experiment results. In the final time frame it can be seen that the the fluid begins to fill a cavity near the wedge. This is a nice indication that the use of spray rails for such geometries are quite necessary. If the fluid were to make contact with the hull, an increased wetted surface resulting in more added resistance would be of consequence.

In the pressure solution, figure (6), a high pressure region travels across the wedge bottom width as the geometry begins to submerge into the fluid. Once the geometry is fully submerged, the interaction area is at its maximum. Therefore, the average pressure on that area decreases which reduces the overall force experienced. As such, the pressure begins to redistribute itself. It can be seen from the final time frame that the largest pressure occurs at the tip of the wedge.

The velocity magnitude can be seen expressed in figure (7). From this it can be seen that as the wedge moves downwards, the air moves at very large velocities to vacate the cavity. Interestingly, as the air is pushed out from under the wedge, a vorticity is formed near the chine. From the final frame it can be seen that the vortex detaches itself, and slowly begins to dissipate. From the final frame it can also be seen that air begins to be encapsulated in the open cavity region. The air here moves at an extraordinary rate to vacate. This cavity collapsing, is due to the stagnation of the wake. The fluid moves quite quickly, however, at a certain point the force of the fluid due to the moving wedge is overcome by the gravitational force. A this point, the fluid takes the path of least resistance and collapses on the open region. These observations are well coupled with figure (8), which shows the velocity vectors of the fluids. In the final frame, a clear detached vortex with a large relative velocity can be confirmed. It also highlights

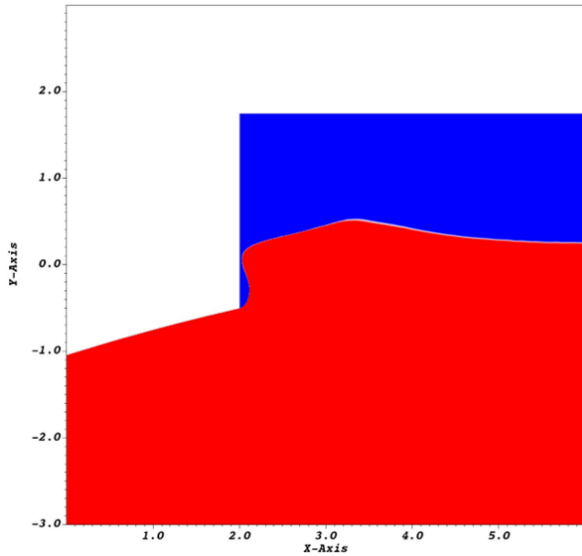
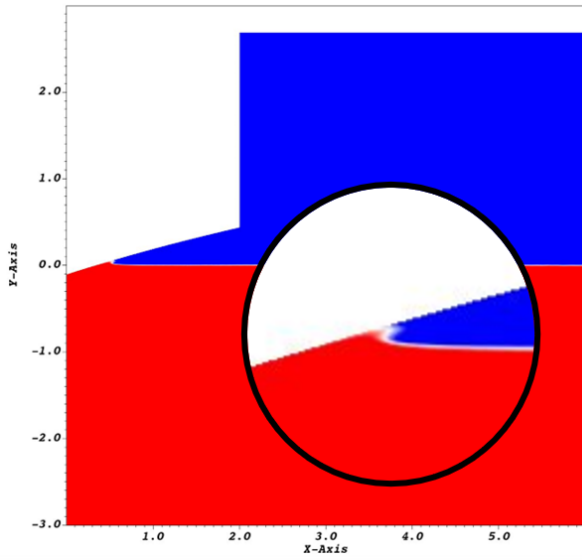


**Figure 5:** Flow solution at  $t = 0.25s$  &  $1.16s$  (102,277 elements)

that the chine region constantly experiences a large region of flow velocities.

#### v. Vertical Force Time Trace

From the output results, a vertical force time trace can be completed on the 2-dimensional wedge. This force is the resulting action due to the impact between wedge and fluid at a constant velocity. The completed time trace for each of the six mesh sizes can be seen in figure (9). The vertical force results indicate a good correspondence with with a decrease in mesh size. It can be seen that the more elements the results begin to overlay one another as an indication of mesh independence. To understand whether this criteria has been achieved a Richardson extrapolation will be performed in Section IV.

From the trace it can be observed that the force lasts for the entirety of the wedge drop simulation. As such, it must clearly be indicated that the wedge should not make contact with the fluid domain until  $t = 0.19s$ . This is clearly illustrated with a vertical line. As such, it is expected that no force should be experienced on the wedge until that time. However, this is not the case. For

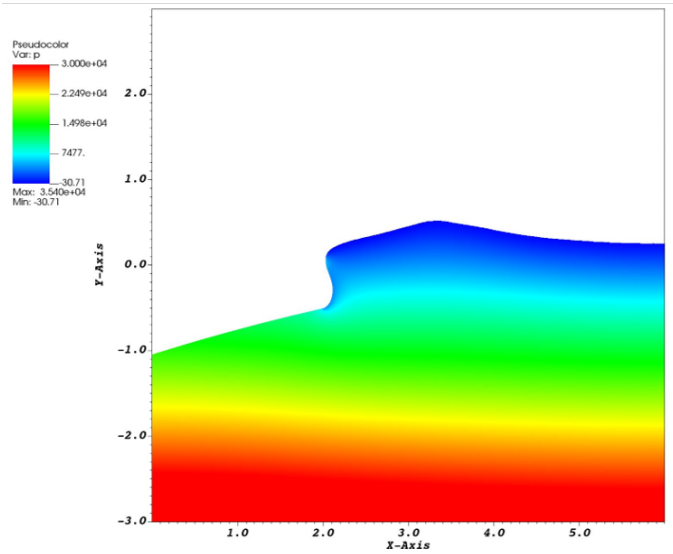
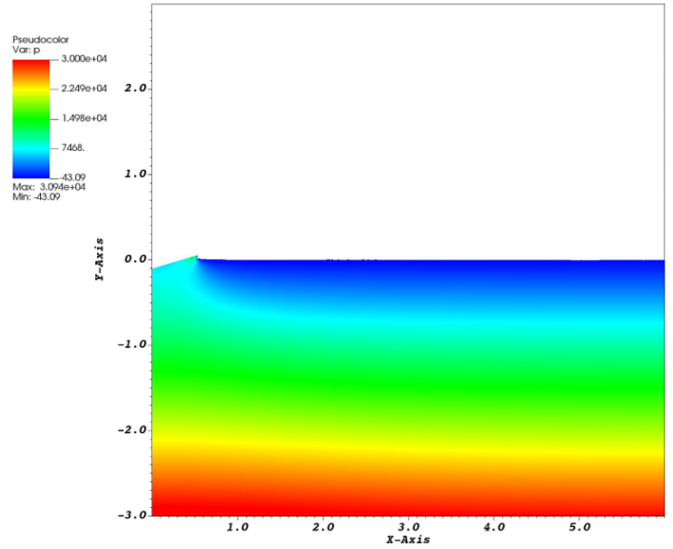


**Figure 6:** Pressure at  $t = 0.25s$  &  $1.16s$  (102,277 elements)

the lowest mesh size there is a clear violation in this result. This is entirely due to the added viscosity in the system. Since the elements are large the effects of viscosity, greatly influences the force experienced well before the wedge enters the fluid. However, for the more refined meshes the elements are sufficiently small to neglect these added effects.

Another interesting observation, is a large vertical force peak presents itself around  $t = 0.5s$ . At this point in time the wedge is nearly completely submerged and the fluid has ramped up along the wedge geometry. A probable cause for such a large peak in the force is due to the large required momentum change necessary to forcibly displace the fluid mass. As the fluid is being moved, the flow is continually accelerating due to the wedge impacting the fluid. Once the wedge is fully in contact the flow does not relatively accelerate much more. This causes a reduction in the overall vertical force. However, this large force causes the fluid to continually move upwards. However, once the wedge is continually submerged, the hydrostatic lifting force is constantly increasing as the wedge descends. This causes an increasing vertical force until the end of the simulation.

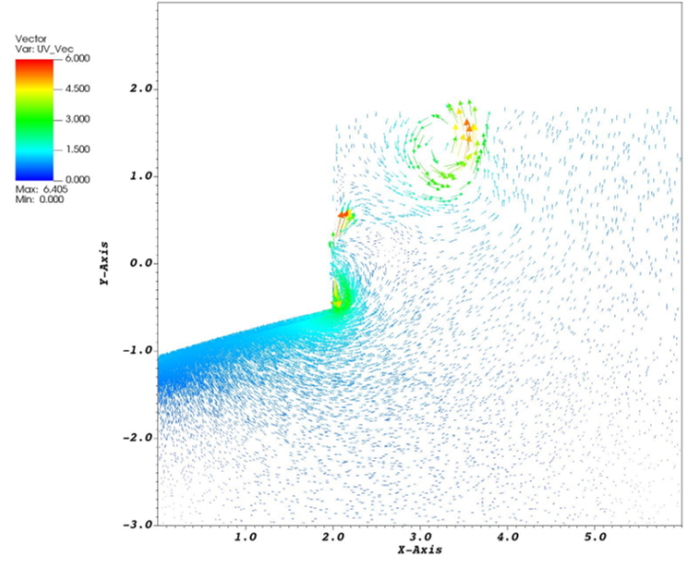
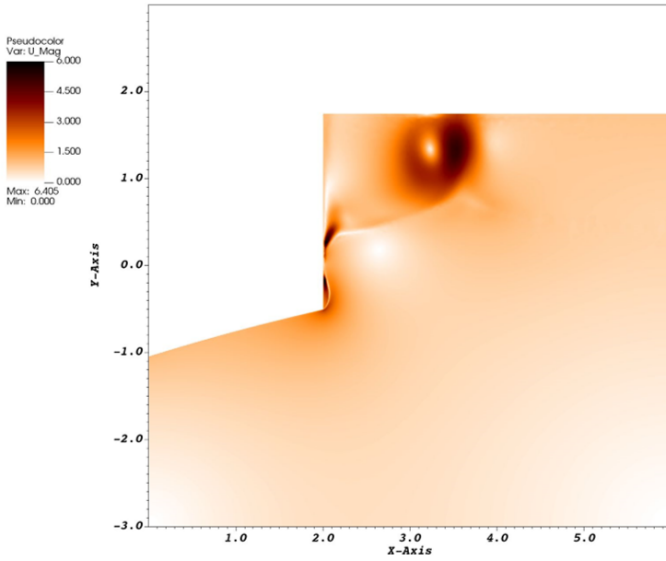
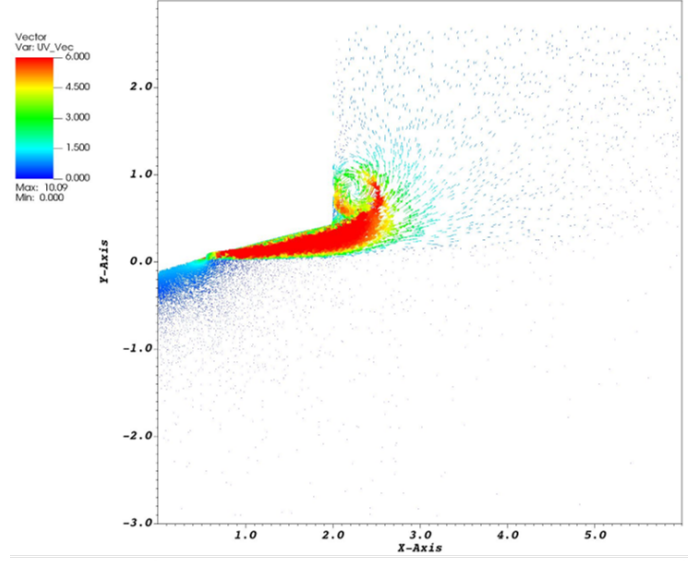
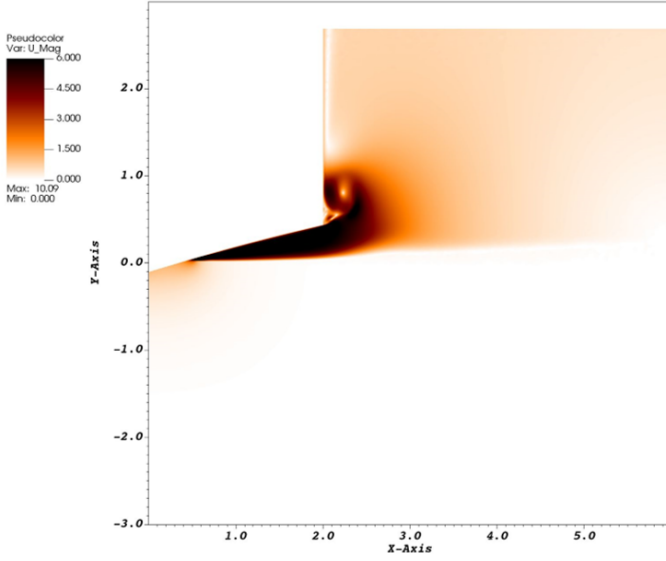


**Figure 7:** Velocity magnitude at  $t = 0.25s$  &  $1.16s$  (102,277 elements)

**Figure 8:** Velocity vector at  $t = 0.25s$  &  $1.16s$  (102,277 elements)

Finally, nearing the end of the simulation the vertical force begins to spike up. This is a strange increase phenomenon, may rather be caused by a simulation error rather than a physical one. The reason for this is because at the end of the simulation, the cavity next to the wedge is starting to fill. This is causing a large region where air is being entrapped. Unfortunately, due to the incompressibility of the fluids, the system may potentially suffer greatly from this event. This can help to possibly explain the sudden jump in force near the end of the results.

#### vi. Force Transformation Routine

To determine the forces acting on the 3-dimensional planing hull, a conversion routine must be implemented. This procedure is necessary to transform the vertical forces acting on the 2D wedge in the time domain to the normal forces acting on the wet keel length of the hull in the 3D domain. A common practice is to introduce a non-dimensional length relation with respect to the beam length. This relation can be seen in equation (14).

$$\lambda = L_k/b \quad (14)$$

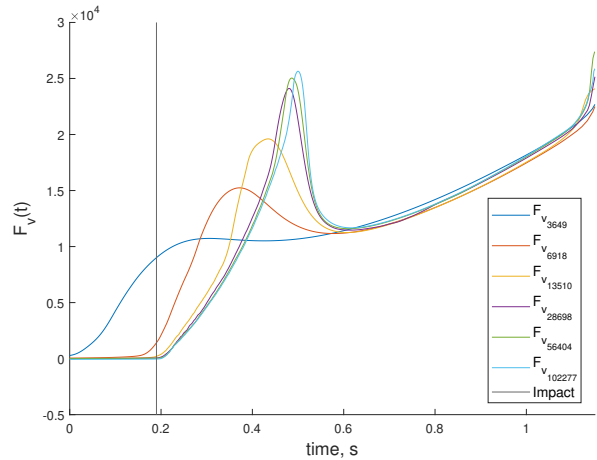


**Figure 9:** Vertical forces in time domain

Where  $L_k$  is the completed wet length of the keel and  $b$  is the beam of the vessel. Before a conversion can occur, the relation

between the time and length domains must be established. This can be done using the governing  $x$ - $t$  relation as seen in equation (1). Using this formulation and trigonometry, the time when the wedge drops through the fluid and the corresponding wet length can be described as,

$$\frac{\lambda}{t_{fluid}} = \frac{U}{b \cdot \cos(\tau)} \quad (15)$$

The 2D vertical force can then be converted into a 3D Normal force by integrating this applied load over the time period of the wedge drop.

$$F_N^{3D}(t) = \int_0^{t_{fluid}} F_V^{2D}(t) dt \quad (16)$$

Then using the relation seen in equation (15), a conversion can be made from the time domain to a normal force with respect to the normalized wetted surface,  $\lambda$ .

$$F_N^{3D}(\lambda) = F_N^{3D}(t) \cdot \left( \frac{U}{b \cdot \cos(\tau)} \right) \quad (17)$$

This integration routine allows for the determination of the singular normal force, from which the lift and drag forces can be determined. These are simply found using the determined trim angle and trigonometric relations as seen below,

$$F_L(\lambda) = F_N(\lambda) \cdot \cos(\tau) \quad (18)$$

$$F_D(\lambda) = F_N(\lambda) \cdot \sin(\tau) \quad (19)$$

A slightly different procedure is required to determining the moment acting with respect to the hull transom.

$$M^{3D}(t) = \int_0^{t_{fluid}} F_V^{2D}(t) \cdot t \cdot \frac{U}{\cos(\tau)} dt \quad (20)$$

Where,  $t$  is the associated time where the distribution is present. These parameters are multiplied by a length conversion to determine the total moment (clockwise positive around the stern) acting on the vessel in the time domain. From there the conversion total length conversion is applied to determine the moment with respect to the keel length.

$$M^{3D}(\lambda) = M^{3D}(t) \cdot \left( \frac{U}{b \cdot \cos(\tau)} \right) \quad (21)$$

Both the normal forces and the moments were both determined in MATLAB using numerical trapezoidal techniques. Having determined the respective lift, drag, and moments, the non-dimensional coefficients can be determined for each. This is achieved using the following relations,

$$C_L(\lambda) = \frac{F_L(\lambda)}{1/2 \cdot \rho \cdot U^2 \cdot S(\lambda)} \quad (22)$$

$$C_D(\lambda) = \frac{F_D(\lambda)}{1/2 \cdot \rho \cdot U^2 \cdot S(\lambda)} \quad (23)$$

$$C_M(\lambda) = \frac{M(\lambda)}{1/2 \cdot \rho \cdot U^2 \cdot S(\lambda) \cdot b} \quad (24)$$

Where,  $S(\lambda)$  is the wetted surface area as a function of the non-dimensional length. This relation can simply be approximated as the total length multiplied by the vessel's beam.

$$S(\lambda) = b \cdot L_k = b^2 \cdot \lambda \quad (25)$$

From equations (22), (23), and (24) plots of the non-dimensional coefficients can be made with respect to the non-dimensionalized wetted keel length. These can be seen in figures (10), (11), and (12) respectively. It should be noted that both the force and surface area is varied as a function of length. Additionally, a Von Karman comparison is plotted. The analytical breakdown of these formulations can be seen in Section (V).

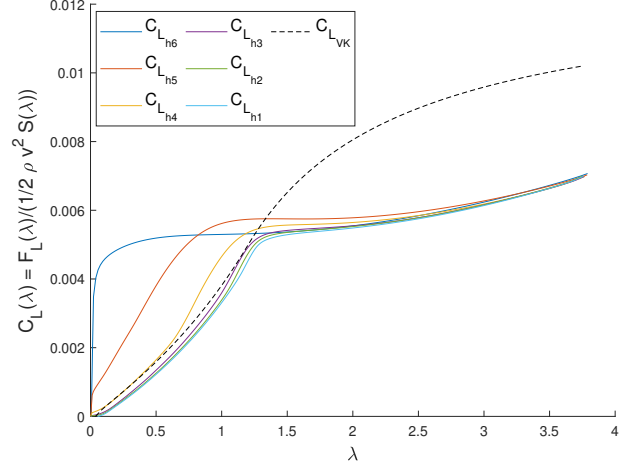


Figure 10: Lift Coefficients as a function of  $\lambda$

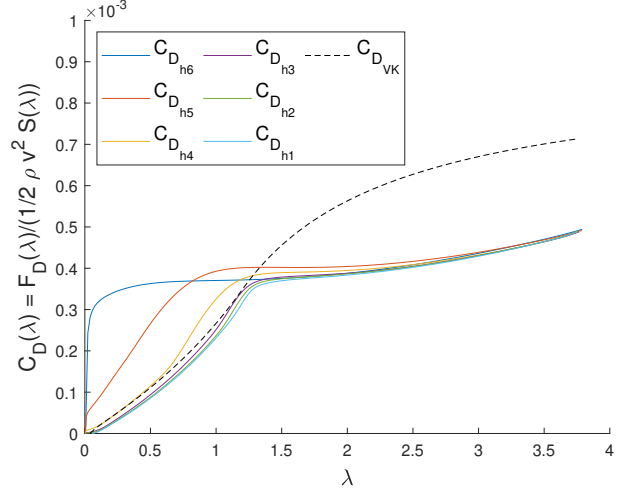


Figure 11: Drag Coefficients as a function of  $\lambda$

## IV. VERIFICATION AND VALIDATION

### i. Richardson Extrapolation

The Richardson Extrapolation technique is a tool which allows for a formal approach to mesh verification. It produces numerical evidence on the quality of the mesh refinement. The analyzed mesh sizes and resulting normal forces corresponding to a wetted keel length of 14.29m can be seen summarized in table (5).

There are four possible error representation options when performing the extrapolation. These include a linear, quadratic, monomial, and polynomial representations. Each of the four assumptions can be used to compute unknown exact coefficients as well as the final exact solution value. Each of the four assumptions will be analyzed and interpreted in relation to one another

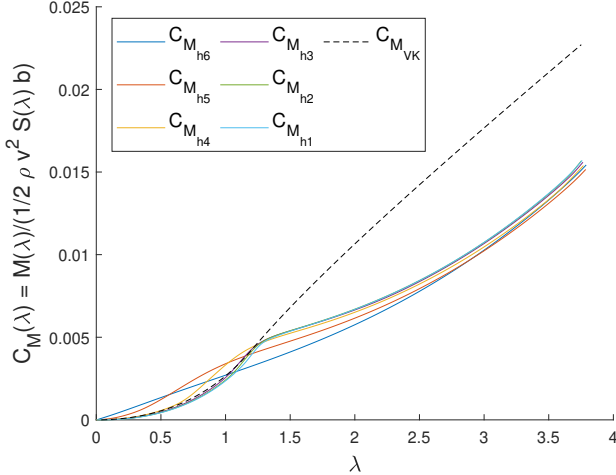


**Figure 12:** Moment Coefficients as a function of  $\lambda$  to identify the best representation.

### 1. 1st order and 2nd order

The linear and quadratic assumptions have a very similar forms. Both representations require the determination of two unknowns. Therefore, these expressions only require two known  $\phi$  parameters to determine constant C and the exact solution  $\phi_0$ . The only difference between the two formulations is the exponent attached to the mesh size. These formulations for linear and quadratic can both be seen below respectively,

$$\phi^h - \phi_0 = C_1 \cdot h \quad (26)$$

$$\phi^h - \phi_0 = C_1 \cdot h^2 \quad (27)$$

Where  $\phi^h$  is the corresponding solution for each corresponding mesh size,  $\phi_0$  is the exact solution determined by the assumption, C is the unknown constant, and h is the respective mesh size to a fixed exponent.

### 2. General monomial

The general monomial assumption differs slightly from the linear and quadratic cases in that instead of an established p, the order of convergence is unknown. Therefore to successfully determine the three unknowns, three input results are required.

$$\phi - \phi^h = C \cdot h^p \quad (28)$$

However, this case also requires very specific criteria to be established to confirm the accuracy of the extrapolation. The first required criteria, is that the mesh ratios must be

**Table 5:** Richardson extrapolation input parameters

Mesh	Element Size	$h_i/h_1$	$F_N$ (kN)
$h_6$	0.0921	5.29	209.8
$h_5$	0.0669	3.85	208.5
$h_4$	0.0478	2.75	206.13
$h_3$	0.0343	1.97	205.9
$h_2$	0.0246	1.41	205.7
$h_1$	0.0174	1.00	205.7

equivalent. This can only done when the meshing is done based on the same geometric family.

$$\frac{h_1}{h_2} = \frac{h_2}{h_3} \quad (29)$$

The next condition that is required is to establish whether monotone convergence occurs. This can be done by taking the equal grid refinement ratios between the medium/fine and coarsest/medium grids. If this ratio is greater than 0 then the apparent convergence of the points behave in a monotonic convergent way.

$$R = \frac{\phi_1 - \phi_2}{\phi_2 - \phi_3} > 0 \quad (30)$$

If both of these criterion are established, the observed order of convergence can successfully be calculated using the following relation,

$$p = \frac{\log(R)}{\log\left(\frac{h_1}{h_2}\right)} \quad (31)$$

If the order of convergence is determined, the unknown constant, C, can be easily determined by taking a difference between two errors which result in the following expression,

$$C = \frac{\phi_1 - \phi_2}{h_1^p - h_2^p} \quad (32)$$

Finally, the exact solution for the most refined mesh size can be determined by implementing the previous solutions,

$$\phi_0 = \phi_1 - C \cdot h_1^p \quad (33)$$

### 3. Polynomial

The final assumption is through the implementation of a polynomial representation.

$$\phi^h - \phi_0 = C_1 \cdot h + C_2 \cdot h^2 \quad (34)$$

Much like the monomial case, this assumption has three unknown parameters. However, unlike the monomial case can easily be solved as a linear system of equations using three known input error formulations for different mesh sizes.

From each of these assumptions a general error and uncertainty can be determined for each mesh size. However, generally it is sufficient to view the smallest determined mesh parameters since it can be anticipated that this will produce both the smallest error and uncertainty. These relations can be seen below in equations (35) and (36) respectively.

$$E_1 = |\phi_0 - \phi_1| \quad (35)$$

$$U_1 = \frac{||\phi_0 - \phi_1||}{||\phi_1||} \quad (36)$$

Using the above assumptions, error, and relative uncertainty formulations all unknowns can be determined for each case. The summary of all the results can be seen in table (6).

**Table 6:** Richardson extrapolation output parameters

	Linear	Quadratic	Monomial	Polynomial
$C_1$	4.9844E3	1.19E5	1.3308E9	-2.863E4
$C_2$	-	-	-	8.01E5
$p$	1	2	4.64	1 & 2
$\phi_0$	2.06E5	2.06E5	2.06E5	2.06E5
$E_1$	86.7	35.9	9.0	255.7
$U_1$	4.21E-4	1.75E-4	4.36E-5	1.20E-3

## ii. Richardson Extrapolation Interpretation

From the extrapolations, a few conclusions can be drawn. The first is that the monomial has the lowest error and uncertainties. However, this is not a true reflection on how the whole data set is fitted. Since the Richardson Extrapolation only considers the last three data points. From that, it can be seen that the true global best fit is from the the polynomial assumption. However, this to has its drawbacks. This extrapolation actually rises slightly at the end of the extrapolation. This is inherently incorrect, since the solution should be of the form monotonic convergence. However, if the first three points are disregarded, then the monomial assumption is ideal. A least squares approximation would be an interesting addition to the verification procedure. This technique incorporates all data and produces a sound procedure to determine uncertainty of the entire data set. Unfortunately, due to time constraints, this procedure was skipped but was still deemed worth mentioning.

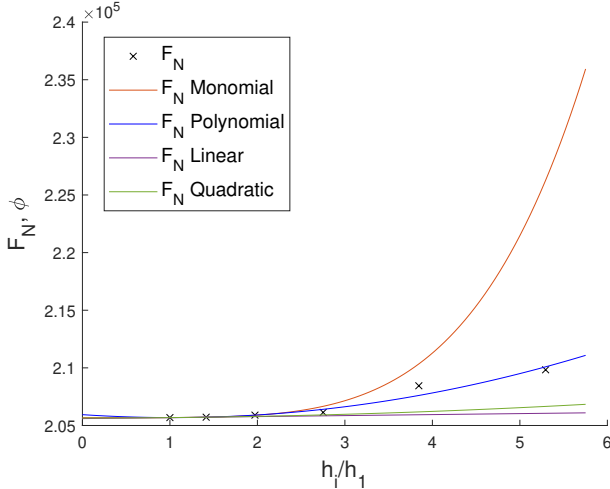


**Figure 13:** Normalized Richardson extrapolations

## V. VON KARMAN ANALYTICAL ANALYSIS

Having verified the results using the Richardson extrapolation, validation of the results can be done through an analytical comparison. To give an indication of the drag and lift in an analytical way, a calculation is done using the Von Karman theorem which is based on the momentum theorem that states that the total momentum of a system will remain constant (neglecting losses) [1]. For this case this means that the original momentum of the vessel will be distributed between the body and the water during impact. During this impact the vessel is simulated as a flat plate (width =  $2R$ ) and the apparent mass of the water ( $M_{water}$ ) and vessel together increases with the amount of fluid contained within half a cylinder below the vessel, see formula (37). The added mass of

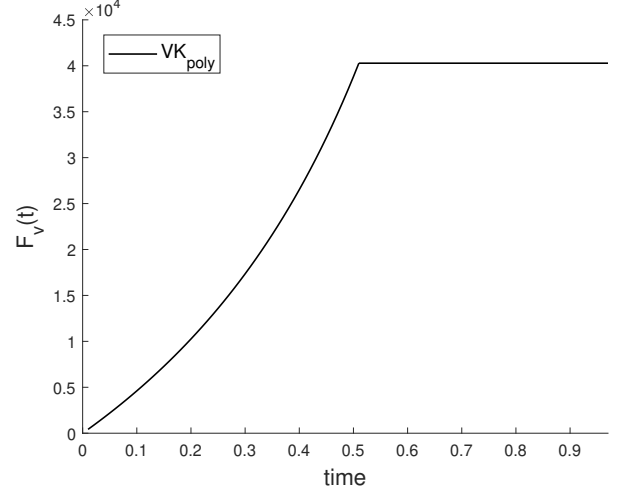


**Figure 14:** Time trace of the entry force on the entire vessel  
the air above the vessel will be neglected.

$$m_{water} = \rho \frac{1}{2} \pi R^2 \quad (37)$$

Furthermore there is also an effect from the buoyancy on the vessel, however this is not taken into account with the Von Karman theorem for vessels with a small deadrise. During the impact of the wedge the vertical velocity will remain constant, therefore the exceeded force on the vessel can be calculated with formula (38). Substituting the change in mass (formula 39) and the derivative of the beam (formula 40) gives the final formula (41).

$$F = \frac{d}{dt}(m_{water} \cdot v) = \dot{m}_{water} \cdot v \quad (38)$$

$$\dot{m} = \rho \pi R \frac{dR}{dy} v \quad (39)$$

$$\frac{dR}{dy} = \frac{1}{\frac{dY_{poly}}{dR}} = \frac{1}{0.0414R + 0.311} \quad (40)$$

$R$ , the varying width of the wedge is also a function of time. Therefore, for each time step radius must be solved using the polynomial expression. Substituting these formulations, force can be determined as,

$$F = \pi \rho \left( \frac{dR}{dy} \right)^2 v_o^3 t \quad (41)$$

Using formula (41) the time trace of the entry force on the vessel is calculated with Matlab, using the parameters as determined earlier with Savitsky (see table (1)) that approximated a depth of  $1.04m$  and a trim of  $4^\circ$ . The result can be seen in figure (14), that shows that a maximum force of  $39 \text{ kN}$  is exerted on the wedge after  $t=0.5s$  when the chine has hit the water. From the time trace the total normal force on the vessel has been calculated using numerical trapezoidal integration in Matlab. The lift and drag have then been determined from the normal force using a similar force transformation and integration technique as seen in Section (vi). The results can be seen in figure (15) as a function of the wetted keel length which gives a drag of  $15.01 \text{ kN}$  and a lift of  $299 \text{ kN}$ . Finally the pitching moment using the similar moment

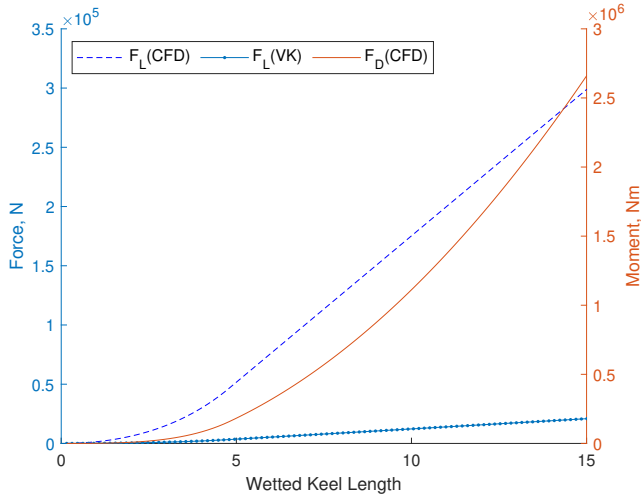


**Figure 15:** Lift, drag and pitching moment as a function of the wetted keel length.

method as the CFD (see formula (20) and (21)) around the stern has been calculated as a function of the wetted keel length. This resulted in a pitching moment of  $2662 \text{ kNm}$ , the full results of the lift, drag, and moment analytical calculations can be seen in figure (15).

## VI. ANALYTICAL COMPARISONS & CONCLUSION

Based on the time-trace values determined from the CFD and Von Karman analysis, a detailed evaluation can be made. The comparison between these results can be seen in figure (16). It can initially be seen that the polynomial incorporated Von Karman provides a large over-estimate as compared to the actual CFD results. The reason for this skewed data, is related to the actual shape of the wedge and the fluid acceleration along the bottom. This case assumes that as the wedge moves down the fluid begins to move up while reaching the same constant drop velocity. This would imply that the wedge geometry is completely in contact with the fluid at  $t = 0.5$ . However, this was clearly not the case. When the wedge impacts fluid, based on the CFD results, it confirms that the fluid actually rises at a much faster rate. This rate corresponds to approximately a 3x larger acceleration as compared to the original constant velocity fluid rise. A Von Karman comparison using this modified acceleration can be seen in figure (16). The correspondence between this result very closely correspond to the CFD as opposed to the initial Von Karman assumptions. A valid explanation of the increased fluid acceleration can be directly related to the wedge geometry. When comparing to a constant deadrise angle, the related maximum results are aligned quite well. However, the peak of the results shift earlier when the polynomial function is implemented. The concave shape must act as a sort of 'ramp' for the fluid to accelerate. Therefore, the basic Von Karman assumptions, without appropriate consideration to the rate of change of the fluid velocity due to geometry, does not correspond well with the expected results.

A comparison between the lift, drag and moment forces can also be evaluated. However, in this case an additional analytical comparison can be made based on the Savitsky results for lift and drag. Overall, the results have generally okay correspon-

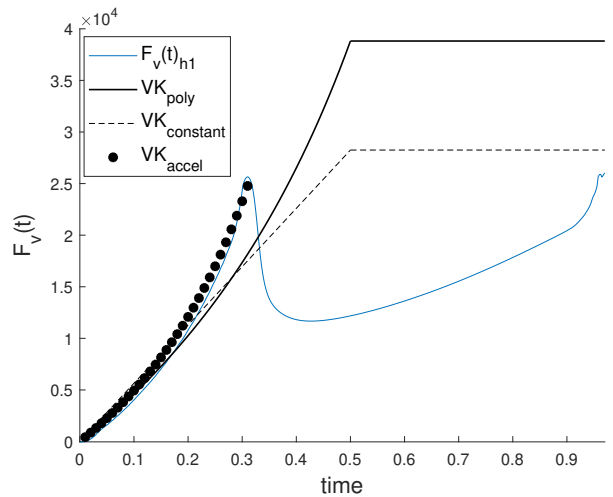


**Figure 16:** Time Trace Comparison

dence, considering that the Von Karman time-trace is greatly over predicted. It should be noted that, the sensitivity between lift and drag relations are very large. It can be seen that while the results for drag are extremely close, the application of converting through the use of the trim angle relation causes a large disparity between the lifting results. This sensitivity in turn greatly effects the moments as well. While the results are not extremely accurate between the CFD, Von Karman, and Savitsky. It can be inferred that for quick, conservative results within the same order of magnitude, these analytical expressions can be extremely useful.

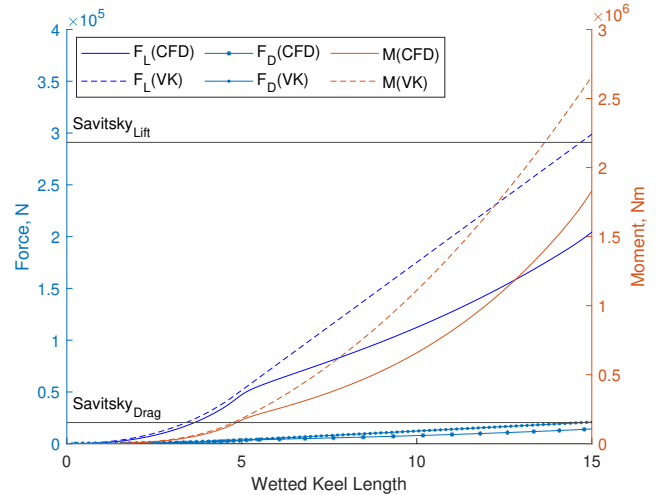


**Figure 17:** Force and Moment Comparisons

## REFERENCES

- [1] Theodore Von Karman. "The impact on seaplane floats during landing". In: *National advisory committee for aeronautics* 1.321 (1929), pp. 1–8.
- [2] Daniel Savitsky. "Hydrodynamic Design of Planing Hulls". In: *Marine Technology* 1.1 (1964), pp. 71–95.